Received: 22 July 2020 | Revised: 8 December 2020 | Accepted: 11 December 2020

IET Optoelectronics

DOI: 10.1049/ote2.12033

The Institution of Engineering and Technology WILEY

ORIGINAL RESEARCH PAPER

# AlGaAs/GaAs asymmetric-waveguide, short cavity laser diode design with a bulk active layer near the *p*-cladding for high pulsed power emission

**Eugene A. Avrutin**[1] | **Boris S. Ryvkin**[2,3] | **Juha T. Kostamovaara**[2]

[1]Department of Electronics, University of York, York, UK

[2]Department of Electrical and Information Engineering, University of Oulu, Oulu, Finland

[3]A F Ioffe Physico-Technical Institute, St. Petersburg, Russia

**Correspondence**

Eugene A. Avrutin, Department of Electronics, University of York, York, YO10 5DD, UK.
Email: eugene.avrutin@york.ac.uk

**Funding information**

Academy of Finland, Grant/Award Number: 317144

**Abstract**

It is shown theoretically that a GaAs/AlGaAs laser diode design using an asymmetric waveguide structure and a bulk active layer (AL), located close to the p-cladding, can provide high output power in a single, broad transverse mode for short-wavelength (<0.9 μm, matching the spectral range of high efficiency of silicon photodetectors) pulsed emission in the nanosecond pulse duration region, typically <<100 ns. The dependences of the laser performance on the thickness of the AL and the cavity length are analysed. It is shown that the relatively thick bulk AL allows the of short cavity lengths (<1 mm), for achieving high pulsed power while maintaining a relatively low series resistance and a narrow far field.

## 1 | INTRODUCTION

High power broad area diode lasers operating in the quasi-continuous-wave (quasi-CW) pulsed regime (with pump pulses long enough to achieve steady state from the laser dynamics point of view yet short enough to not cause substantial current heating, in practice corresponding to the nanosecond region) are important components of Lidars [1] as well as for a number of other applications. With regard to the spectral range of laser emission, two strategies are possible. One involves working in the eye-safe spectral range of 1300–1600 nm, allowing high output power to be used, and requiring InGaAsP/InP [2–4] or AlGaInAs/InP [5–9] based sources and photodetectors. The other involves working at shorter wavelengths and can be further subdivided in two spectral regions: $\lambda \sim 0.9$–$1.1$ μm [10–13] and $\lambda < 0.9$ μm, used [14, 15] for the case of nanosecond pump pulses resulting in picosecond pulse emission under gain-switched operation. The latter spectral range makes use of the efficient and reliable GaAs/AlGaAs emitters and, crucially, the relatively mature technology of Silicon Single-Photon Avalanche Photodetectors [16] which have a high sensitivity at the operating wavelengths below 900 nm.

Traditionally, the design of high-power laser structures in both InGaAsP/InP and (InGaAs)GaAs/AlGaAs material systems used almost exclusively thin active layers (ALs), including 1–3 Quantum Wells (QWs). In the latter case, this was at least because the research largely concentrated on the $\lambda = 0.9 - 1.1$ μm range, where the use of Indium containing components is necessary and growing thick ALs is impossible due to lattice mismatch induced strain. For lattice matched structures, such as In-free GaAs/AlGaAs system and the eye-safe wavelength InGaAsP/InP lasers, there is no such technological limitation. Hence in our work, asymmetric laser designs with a *bulk* AL in a gain-switched GaAs/AlGaAs $\lambda \approx 0.85$ μm laser [14, 15] and, later, in a quasi-CW operated InGaAsP/InP $\lambda \approx 1.5$ μm devices [3, 4, 17] have been proposed and realised. The results on the long-wavelength lasers compared favourably with the best published results, with considerable scope for further optimisation. Here, we show that the same strategy can also be applied in the design of quasi-CW operated GaAs/AlGaAs lasers, compatible with silicon photodetectors.

## 2 | STRUCTURE

The logic behind the structure design is the same as used earlier (Refs. [3, 4, 18] and references therein) in the work long-

wavelength lasers. The most important parameter to be maximised in high-power lasers is the quantum efficiency, which is the product of injection and output efficiencies: $\eta = \eta_i \eta_{out}$. Some compromise in the form of an increased threshold current may be required, and is justified in order to achieve an increased $\eta$, so long as the threshold increase is not drastic.

In modern laser structures, the leakage of electrons into the *p*-cladding is very small so that the injection efficiency, at not-too-high temperatures, can be $\eta_i \approx 1$ [10]. The goal then becomes increasing with the output efficiency $\eta_{out} = \frac{\alpha_{out}}{\alpha_{out}+\alpha_{in}}$, $\alpha_{in}$ and $\alpha_{out} = \frac{1}{2L}\ln\frac{1}{R_{HR}R_{AR}}$ being, respectively, the internal optical losses and the outcoupling losses, $R_{HR}$ and $R_{AR}$ standing for the high-reflection and anti-reflection coated facet reflectances, respectively. Substantial research effort has gone into minimising $\alpha_{in}$ both near the threshold [10, 19, 20] and at high injection level (see e.g. [17, 21–23]). A potentially very efficient complementary way of increasing $\eta_{out}$ in pulsed lasers is to reduce the effect of $\alpha_{in}$ by decreasing the cavity length $L$ and hence increasing $\alpha_{out}$. However, if the thickness of the active region and, accordingly, the confinement factor of the active region ($\Gamma_a$), are small, the decreased $L$ can drastically increase the threshold carrier density $N_{th}$. If this parameter is allowed to reach values of $N_{th} \sim 10^{19}$ cm$^{-3}$, in addition to the risk of compromising the threshold current beyond the acceptable level, the carrier escape from the active region into the OCL-layer by increasing $\alpha_{in}$ and thus compromising $\eta_{out}$, as well as current leakage into the *p*-cladding affecting $\eta_i$, can become significant even at room temperatures.

Thus, efficient operation of a short cavity laser with the AL near the *p*-cladding as in Figure 1a is possible only with an active region of a relatively large thickness ($d_a \sim 1000$ Å in the case under consideration) and the corresponding substantial value of $\Gamma_a$, avoiding excessive increase in $N_{th}$. In principle, this can be either a bulk or Multiple Quantum Well (MQW) structure. However, for a given total thickness $d_a$ of the AL, the bulk AL gives a larger overlap with the purely *active* material than the MQW, in which some of the AL is occupied by the barriers between the wells.

Thus, the design proposed, like that of the long-wavelength laser [3,4, 17, 18], is intended to use a bulk AL to provide substantial values of $\Gamma_a$, whilst keeping $\alpha_{in}$ relatively low. The limit to how short the cavity can be, assuming quasi-CW operation without heating can be ensured, is set by the requirement that $N_{th}$ is not excessively high.

The proposed laser waveguide structure is shown in Figure 1a.

As in the work on long-wavelength lasers [18], the doping levels and thicknesses of the layers of the structure are selected to obtain high injection efficiency, low $\alpha_{in}$ at both low and high injection levels, minimum series and thermal resistances. Most importantly, minimising the modal overlap with the *p*-cladding (to ensure low $\alpha_{in}$ at low injection) requires a substantial refractive index step at the *p*-OCL/*p*-cladding interface, whereas avoiding a strong carrier accumulation and $\alpha_{in}$ increase at high injection levels means that the distance between the AL and the *p*-cladding needs to be small. To further decrease the carrier accumulation in the OCL, high doping of

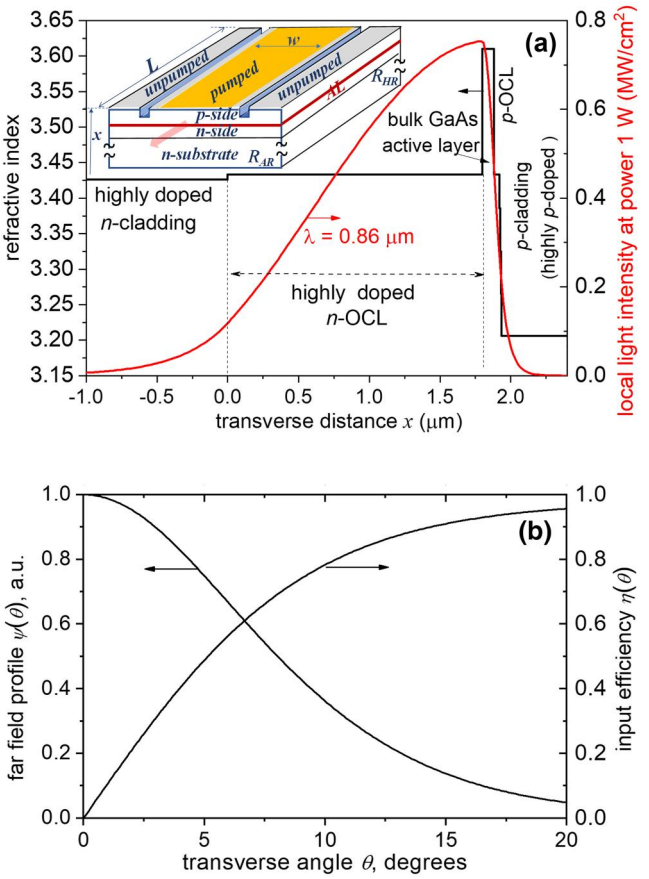


**FIGURE 1** (a) Schematic of the laser structure and the waveguide mode intensity distribution and (b) the corresponding far field of the laser emission and fast-axis waveguide input efficiency. Stripe width $w = 100$ μm, active layer thickness $d_a$=800 Å. The inset to Figure 1a shows a typical 3D structure possible, with the *n*-side comprising the *n*-cladding and the *n*-emitter and the *p*-side, the *p*-cladding and the *p*-emitter

the *n*-OCL can be used [17, 18], which is one of the differences between the current design and the gain-switched one of [14, 15] (the other one being the position of the AL with respect to the peak of the modal profile, which is optimised somewhat differently for gain-switched and quasi-CW applications). Furthermore, a small refractive index step at the *n*-OCL/*n*-cladding interface provides good fundamental mode selection (see below) and a broad near field fundamental ($TE_0$) mode distribution (quantified by the modal field profile $\psi_0(x)$ or a modal intensity profile $\psi_0^2(x)$, also illustrated in Figure 1a). This makes for a narrow far field

$$\Psi(\theta) \propto \left| \int_{-\infty}^{\infty} \psi_0(x) e^{jk \sin\theta} dx \right|^2 \cos^2\theta, \; k = 2\pi/\lambda,$$

and hence potentially high brightness. This is illustrated in Figure 1b which shows the far field $\Psi(\theta)$ as well as the efficiency $\eta$ of coupling the light into a given one-dimensional numerical aperture $\theta$ (in this case, this may approximately represent the LIDAR collimation optics) estimated as $\eta(\theta) = \int_0^{\theta} \Psi(\vartheta) d\vartheta / \int_0^{\pi/2} \Psi(\vartheta) d\vartheta$.

The parameters that were fixed in the studies below were the refractive index steps, the thicknesses of *n*-OCL and *p*-OCL layers ($d_{n\text{-}OCL}$ = 1.8 μm >> $d_{p\text{-}OCL}$ = 0.04 μm as in Figure 1), and the doping levels of the layers, in particular $N_D^{(n-OCL)} = N_D^{(n-clad)} = 1 \times 10^{18}$ cm$^{-3}$. The parameters that were varied were the width of the AL $d$ and the cavity length $L$.

## 3 | ANALYSIS OF LASER PERFORMANCE

We first analyse the threshold behaviour of the laser.

Similarly, with regard to long-wavelength lasers [18], we consider pulsed (quasi-CW) operating regime, with the injection current pulse short enough (<<100 ns) to not cause appreciable laser heating, as is typically the case in LIDAR applications. Thus room-temperature dependences of peak gain $g$ on carrier density $N$ can be used in calculations. To analyse what may be, in general, large variations of the threshold carrier density $N_{th}$, we use the three-parameter logarithmic gain-carrier density dependence $g(N) = G_0 \ln\frac{N+N_1}{N_{tr}+N_1}$ [24] , rather than the simpler linear approximation used in [17, 18] following [25]. Then, the threshold carrier density is determined from the transcendental equation

$$N_{th} = (N_{tr} + N_1)\exp\frac{\alpha_{in}^{(th)}(N_{th}) + \alpha_{out}}{\Gamma_a G_0} - N_1 \qquad (1)$$

where, as in [17, 18], the internal losses at threshold contain just two contributions

$$\alpha_{in}(i, N) \approx \alpha_{in}^{(\text{built-in})} + \alpha_{AL}^{(\text{FC})}(N_{th}) \qquad (2)$$

The first term in Equation (2) is the built-in losses $\alpha_{in}^{(\text{built-in})} \approx 3.0\text{cm}^{-1}$, of which the main part (≈2.6 cm$^{-1}$ for $d_a$ = 800 Å as in Figure 1) is associated with free carrier absorption in the doped *n*-OCL and *n*-cladding, calculated using the modal profile of Figure 1 and the common doping level $N_D = 10^{18}$ cm$^{-3}$; the rest accounts for the (weak) overlap of the mode with the (also highly doped) *p*-OCL and *p*-cladding. This is quite different from earlier work on InGaAsP materials, in which the *n*-doped layers made very little contribution to $\alpha_{in}^{(\text{built-in})}$ due to the very low values of the free-electron absorption cross-section in those materials. The second term in Equation (2) is the free carrier absorption in the AL at threshold

$$\alpha_{AL}^{(\text{FC})}(N_{th}) = \Gamma_a(\sigma_{ea} + \sigma_{ha})N_{th} \qquad (3)$$

where $\sigma_{ea}$ and $\sigma_{ha}$ are free electron and free hole absorption cross-section in the AL material. Similar to the previous work, Equation (2) neglects the presence of non-equilibrium carriers in all the non-active parts of the waveguide, which is justified at the relatively low threshold current.

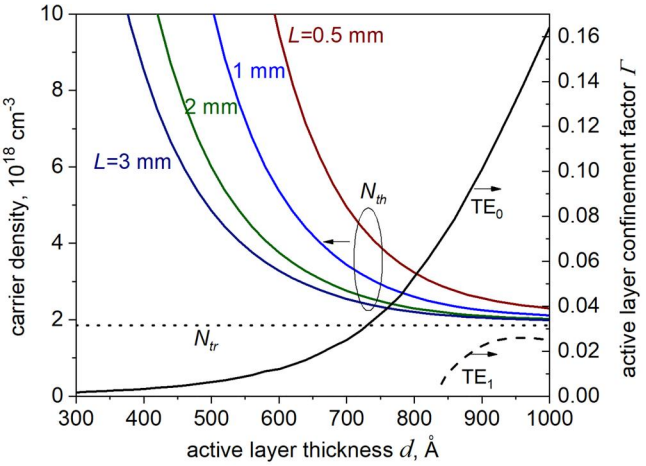


**FIGURE 2** Confinement factor $\Gamma_a$ and active layer carrier densities for different cavity lengths as functions of the active layer thickness $d_a$. Other waveguide parameters as in Figure 1; *n*-side doping $N_D^{(n-OCL)} = N_D^{(n-cl)} = 1\times10^{18}$ cm$^{-3}$

Figure 2 shows the calculated value of the confinement factor $\Gamma_a$, as well as the threshold current density for several values of the cavity length $L$, as functions of the AL thickness $d_a$. For a thin AL ($d_a$ <∼ 400 Å), the value of $\Gamma_a$ is approximately proportional to $d_a$; for thicker AL, the dependence $\Gamma_a(d_a)$ becomes super-linear reflecting the increasingly important waveguiding properties of the AL itself. At $d_a$ >∼ 900 Å, the waveguide is, strictly speaking, not in a single mode, but the calculated confinement factor for the second (TE1) mode (shown as a dashed line in the figure) is much smaller than that of the fundamental TE0 mode, so there is never any doubt about the single transverse mode operation of this structure.

As can be expected from Equation (1), the strongly increasing $\Gamma_a$ leads to a dramatic decrease in the threshold carrier density with increasing $d_a$; for the shortest cavity analysed ($L$ = 0.5 mm) the value of $N_{th}$ at $d_a$ = 800 Å (as in Figure 1) is substantial but realistic whereas $d_a$ <∼ 600 Å makes $N_{th}$ for such a short cavity impractically high. For longer cavities ($L$ = 1–3 mm), starting with $d_a$ ≈ 600–700 Å and greater, the main contribution to the threshold carrier density is the transparency carrier density $N_{tr} = 1.85 \times 10^{18}$ cm$^{-3}$ [24] ($N_{th} - N_{tr} < N_{tr}$).

We proceed next to analyse the power output of the laser. Similar to the previous work, [3, 17, 18] the light-current characteristics $P(I)$ was calculated self-consistently alongside the power-dependent internal loss $\alpha_{in}(I, P(I))$ and the effective threshold current $I_{th}(I)$, using the transcendental equation

$$P(I) = \eta_i\frac{\hbar\omega}{e}\frac{\alpha_{out}}{\alpha_{out} + \alpha_{in}(I, P(I))}(I - I_{th}(I)) \qquad (4)$$

Here, similar to the previous work, $I_{th}(I) = I_{th}(N_{th}(I))$ is the current expended on creating the AL carrier density $N_{th}(I)$ necessary for the gain to compensate the total losses $\alpha_{out} + \alpha_{in}(I, P(I))$, and the internal loss $\alpha_{in}(I, P(I))$ is calculated using the approach of Equation (2) with added

contributions due to the direct $\alpha_{TPA}^{(\mathrm{mod})}(P(I))$and indirect $\alpha_{TPA}^{(\mathrm{FC})}(P(I))$ two-photon absorption as well as the current-induced carrier accumulation in the OCL $\alpha_j^{(\mathrm{FC})}(I)$:

$$\alpha_{in}(I,P(I)) \approx \alpha_{in}^{(\mathrm{built-in})} + \alpha_{AL}^{(\mathrm{FC})}(N_{tb}(I)) + \alpha_j^{(\mathrm{FC})}(I) + \alpha_{TPA}^{(\mathrm{FC})}(P(I)) + \alpha_{TPA}^{(\mathrm{mod})}(P(I)) \quad (5)$$

The details of calculating individual contributions are described in [17]. An important difference from the numerical results of [17, 18] (which dealt with InGaAsP materials), is the more complex effect of high *n*-doping of the *n*-OCL ($N_D = 10^{18}$ cm$^{-3}$) in the current study. As already mentioned above, the fact that in AlGaAs materials the free-electron absorption cross-section is smaller than the free-hole value by only a factor of ≈3 (as opposed to more than an order of magnitude difference in InGaAsP materials) means that the heavy *n*-doping of the *n*-OCL leads to a substantial $\alpha_{in}^{(\mathrm{built-in})}$. Thus at modest injection levels, the predicted power output of lasers studied here is *below* those with lightly doped *n*-OCL (in which $\alpha_{in}^{(\mathrm{built-in})}$ may be down to <0.5 cm$^{-1}$) However, at high currents, the high level of *n*-OCL doping makes for strong suppression of $\alpha_j^{(\mathrm{FC})}(I)$ (which is important for lasers with a small cavity length *L*, since $\alpha_j^{(\mathrm{FC})}(I)$ scales with the current *density* $j = I/(wL)$) and also to some (modest) extent reduces $\alpha_{TPA}^{(\mathrm{FC})}(P(I))$ [16]. Thus, at $I >\sim$ 40–50 A, the *n*-doping of the *n*-OCL becomes beneficial.

These considerations are illustrated in Figure 3, which shows the current dependences of the total internal loss as well as the contributions to it for the case of high (Figure 3a) and low (Figure 3b) *n*-OCL doping.

As in [3,4], the *p*-OCL contribution to the current-induced carrier absorption $\alpha_j^{(\mathrm{FC})}(I)$ is negligible because of the strongly asymmetric AL position (very thin *p*-OCL). In its absence, other mechanisms of absorption become important. In the design with a low $N_D^{(n-OCL)}$ (Figure 3b), the current-induced carrier absorption in the *n*-OCL $\alpha_j^{(\mathrm{FC})}(I)$ dominates at high currents as discussed above; in the structure with a highly doped n-OCL (Figure 3a) this contribution, too, is suppressed by doping, at the expense of a higher built-in loss as discussed above. Also, important is the indirect TPA effect which is of a similar magnitude in both designs. Note that, in spite of a substantially smaller value of the TPA coefficient in AlGaAs OCL ($\beta_{2,OCL} = 1 \times 10^{-8}$ cm/W [26]) as compared with the value in InGaAsP OCL ($\beta_{2,OCL} = 6 \times 10^{-8}$ cm/W [27]), the TPA effects remain significant in the lasers studied here due to the large intracavity powers generated.

At $I \sim$ 100 A, the laser with a large $N_D^{(n-OCL)}$ has an advantage of about 5%–7% in power output over that with a lightly doped *n*-OCL; both are predicted to achieve power outputs that compare favourably with the results in the literature.

As was anticipated, despite the non-linear loss increase being somewhat higher in the shorter laser cavities, the increase

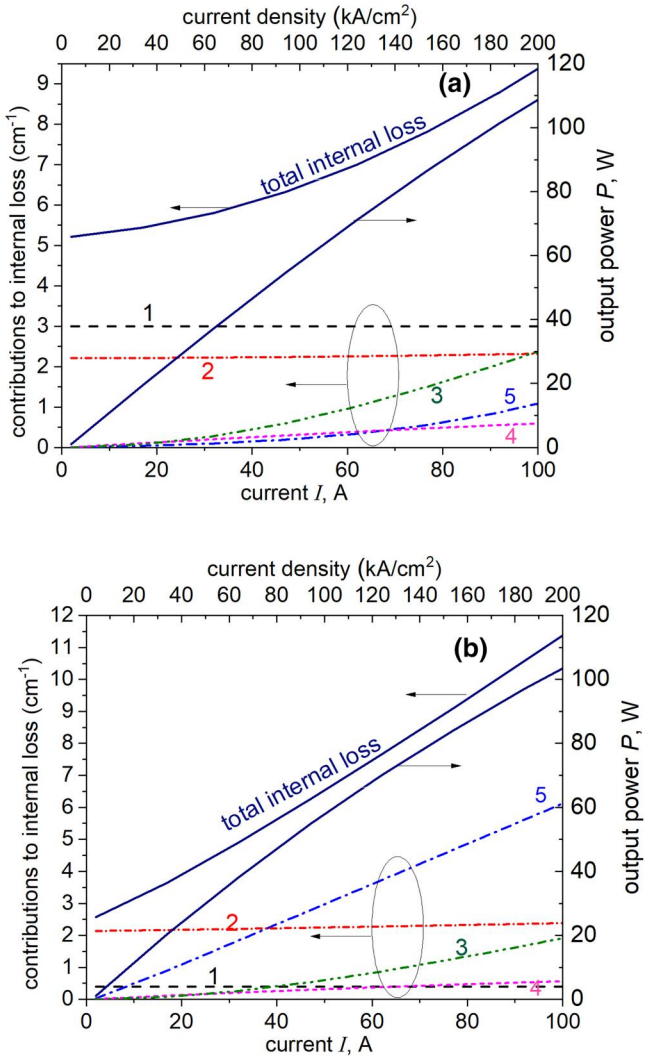


**FIGURE 3** (a) Calculated output power, total internal loss and its individual components as functions of current: $\alpha_{in}^{(\mathrm{built-in})}$(1), $\alpha_{active}^{(\mathrm{FC})}(I)$ (2), $\alpha_{TPA}^{(\mathrm{FC})}(P(I))$(3), $\alpha_{TPA}^{(\mathrm{mod})}(P(I))$(4), $\alpha_j^{(\mathrm{FC})}(I)$ (5). $L$ = 0.5 mm; the waveguide parameters as in Figure 1. Also shown is the output power. (b). As in (Figure 3a), with low n-OCL doping ($N_D^{(n-OCL)} \sim 10^{16}$ cm$^{-3}$)

of $\eta_{out} = \frac{\alpha_{out}}{\alpha_{out}+\alpha_{in}}$ by decreasing the cavity length is a robust enough mechanism of increasing the power output to ensure a substantial (up to >50%) advantage of power output from a laser with $L$ = 0.5 mm at high currents over the lasers with longer cavities as illustrated in Figure 4.

The absolute values of the predicted output power at $I$ = 100 A reach more than 100 W for short cavities ($L$ = 0.5 mm), whereas for the relatively long 3 mm cavity, the value is about 60 W. The latter is similar to the 50 W achieved experimentally at similar currents in an advanced wavelength stabilised $\lambda$ = 905 nm laser (with the same stripe width of $w$ = 100 μm) utilising an asymmetric structure with a Single Quantum Well AL [13].

We note finally that, although the absolute values of *output power* discussed above are the most important advantage for LIDAR applications, the proposed structure design can be

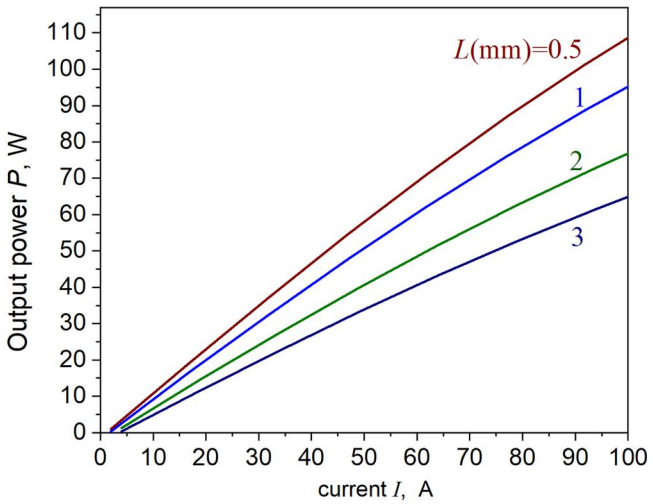


**FIGURE 4** Calculated output power for different cavity lengths. The stripe width $w = 100$ $\mu$m; the waveguide parameters as in Figure 1

expected to decrease the *series resistance* of the device also, and hence its *wall-plug efficiency*, compared to many currently used designs. This is, firstly, because the bulk AL can be expected to virtually eliminate the recently put forward [28] extra series resistance mechanism which is associated with finite capture time in QWs and determined essentially by the excess density of OCL carriers $N_{bj}$ due to the finite capture time $\tau_{cap}$, evaluated [28, 29] as $N_{bj} \approx \frac{j}{ed_a}\tau_{cap} = \frac{I}{ewLd_a}\tau_{cap}$, where $j$ is the current density and $w$ the stripe width. Indeed, in case of a bulk heterostructure, besides the straightforward effect of a lower $N_{bj}$ due to the larger $d_a$, a lower $N_{bj}$ can also be expected due to the fact that $\tau_{cap}$ is identified as just the time of carrier thermalisation, which is well known to be sub-picosecond and thus substantially shorter than $\tau_{cap}$ in QW structures (which depend in a complex way on the QW parameters [30, 31] and can reach picosecond values [28, 31]). The second reason for the reduced series resistance is that the high $n$-OCL doping reduces the resistance of the thick $n$-OCL. Both effects are most pronounced at low to moderate currents—in the case of the OCL resistance effect, this is because the OCL resistance in weakly to moderately doped structures is non-linear, decreasing with the current so that at very high injection levels, the layer doping level makes relatively little difference [32]. A qualitatively similar non-linearity was also established for the extra resistance because of finite capture time [28].

## 4 | CONCLUSIONS

We have analysed the design of single transverse mode AlGaAs/GaAs $\lambda \approx 850$ nm diode lasers with an asymmetric resonator and a bulk AL located very near the $p$-cladding for high-power pulsed (quasi-CW) operation. It was shown that optimisation of power output at high currents can be achieved using short cavity lengths, and also, to a smaller extent, by high $n$-doping of the $n$-side of the waveguide.

## ACKNOWLEDGEMENT

This work was supported by the Academy of Finland under contract 317144.

## REFERENCES

1. Molebny, V., et al.: Laser radar: from early history to new trends. In: Proceedings of SPIE 7835, Toulouse, pp. 7835023. (2010)
2. Boucher, J.F., Callahan, J.J.: Ultra-high-intensity 1550nm single junction pulsed laser diodes. In: Proceedings of SPIE 8039, Orlando, pp. 80390B (2011)
3. Hallman, L.W., et al.: High power 1.5 μm pulsed laser diode with asymmetric waveguide and active layer near $p$-cladding. IEEE Photon Technol. Lett.. 31(30), 1635–1638 (2019)
4. Hallman, L.W., et al.: Double asymmetric structure 1.5μm high power pulsed laser diodes. In: Proceedings of 2019 IEEE Conference on High Power Laser Diodes and Systems (HPD), Coventry, pp. 19–20.IEEE (2019)
5. Marmalyuk, A.A., et al.: Semiconductor AlGaInAs/InP lasers with ultra-narrow waveguides. Quantum Electron. 47(3), 272–274 (2017)
6. Marmalyuk, A.A., et al.: Effect of the waveguide layer thickness on output characteristics of semiconductor lasers with emission wavelength from 1500 to 1600 nm. Quantum Electron. 48(3), 197–200 (2018)
7. Tanbun-Ek, T., et al.: High power diode laser pump sources in the 1.2–1.9 μm range. In: Proceedings of 2019 IEEE Conference on High Power Laser Diodes and Systems (HPD), Coventry, pp. 15–16.IEEE (2019)
8. Tanbun-Ek, T., et al.: Advancements in broad area InP based high power lasers operating from 1100 nm to 2100 nm. In: IEEE International Semiconductor Laser Conference, San Diego, 16–19 Sept 2018, IEEE, Piscataway, NJ pp. 119–120 (2018). https://www.researchgate.net/publication/332530615_Advancements_in_broad_area_InP_based_high_power_lasers_operating_from_1100_nm_to_2100_nm
9. Higa, Y., et al.: High power, 14xx-nm eye-safe, epitaxially stacked pulse laser for detection and ranging applications. In: Proceedings of IEEE Conference on Semiconductor Lasers (ICLC), Santa Fe, pp. 237–238. IEEE (2018)
10. Pikhtin, N.A., et al.: 16W continuous-wave output power from 100 μm-aperture laser with quantum well asymmetric heterostructure. Electron Lett. 40(22), 1413–1414 (2017)
11. Wang, X., et al.: Root-cause analysis of peak power saturation in pulse-pumped 1100 nm broad area single emitter diode lasers. IEEE J. Quantum Electron. 46(5), 658–665 (2010)
12. Veselov, D.A., et al.: Saturation of light–current characteristics of high-power lasers (λ = 1.0–1.1 μm) in pulsed regime. Quantum Electron. 44(11), 993–996 (2014)
13. Knigge, A., et al.: Wavelength-stabilized high-pulse-power laser diodes for automotive LiDAR. Phys. Status Solidi. 215(8) (2018). article 1700439
14. Ryvkin, B.S., et al.: Asymmetric-waveguide laser diode for high-power optical pulse generation by gain switching. IEEE/OSA J. Lightwave Technol. 27(12), 2125–2131 (2009)
15. Lanz, B., et al.: Performance improvement by a saturable absorber in gain-switched asymmetric-waveguide laser diodes. Opt. Express. 21(24), 29780–29791 (2013)
16. Pancheri, L., Stoppa, D.: Low-noise CMOS single-photon avalanche diodes with 32 ns dead time. In: Proceedings of 37th European Solid State Device Research Conference, Munich, 11–13 Sept 2007, pp. 362–365. IEEE (2007)
17. Ryvkin, B.S., et al.: Strong doping of the $n$-optical confinement layer for increasing output power of high- power pulsed laser diodes in the eye

safe wavelength range. Semicond. Sci. Technol. 32(12) (2017). paper 125008
18. Ryvkin, B.S., et al.: Asymmetric-waveguide, short cavity designs with a bulk active layer for high pulsed power eye-safe spectral range laser diodes. Semicond. Sci. Technol. 35(2020), 085008 (2017)
19. Slipchenko, S.O., et al.: Ultralow internal optical loss in separate confinement Quantum Well laser heterostructures. Semicond. 38(12), 1430–1439 (2004)
20. Gokhale, M.R., et al.: High-power high-efficiency 0.98-mm wavelength InGaAs-(In)GaAs(P)-InGaP broadened waveguide lasers grown by gas source molecular beam epitaxy. IEEE J. Quantum Electron. 33(12), 2266–2276 (1997)
21. Crump, P., et al.: Efficient high-power laser diodes. IEEE J. Sel. Top. Quantum Electron. 19(4) (2013). article 1501211
22. Hasler, K.H., et al.: Comparative theoretical and experimental studies of two designs of high-power diode lasers. Semicond. Sci. Technol. 29(4) (2014). article 045010
23. Ryvkin, B.S., Avrutin, E.A.: Asymmetric, nonbroadened large optical cavity waveguide structures for high-power long-wavelength semiconductor lasers. J. Appl. Phys. 97(11) (2005). article 123103
24. Coldren, L.A., et al.: Diode Lasers and Photonic Integrated Circuits. Wiley, New York (2012)
25. Leuthold, J., et al.: Material gain of bulk 1.55 mu m InGaAsP/InP semiconductor optical amplifiers approximated by a polynomial model. J. Appl. Phys. 87(1), 618–620 (2000)
26. Dogan, M., et al.: Two photon absorption in high power broad area laser diodes. Proc. SPIE. 8965, 896501-896507 (2014)
27. Juodawlkis, P.W., et al.: Continuous-wave two-photon absorption in a Watt-class semiconductor optical amplifier. Opt. Express. 16(16), 12387–12396 (2008)
28. Boni, A., et al.: Impact of the capture time on the series resistance of quantum-well diode lasers. Semicond. Sci. Technol. 35 (2020). article 106484
29. Avrutin, E.A., Ryvkin, B.S.: Theory of direct and indirect effect of two-photon absorption on nonlinear optical losses in high power semiconductor lasers. Semicond. Sci. Technol. 32(1), 015004 (2017)
30. Hader, J., et al.: Structural dependence of carrier capture time in semiconductor quantum-well lasers. Appl. Phys. Lett. 85(3), 369–371 (2004)
31. Abakumov, V.N., et al.: Nonradiative Recombination in Semiconductors. Nuclear Physics Institute, St.Petersburg (1997). Chapter 13 (in Russian)
32. Avrutin, E.A., Ryvkin, B.S.: Dember type voltage and nonlinear series resistance of the optical confinement layer of a high-power diode laser. J. Appl. Phys. 113(4) (2013). article 113108

**How to cite this article:** Avrutin, E.A., Ryvkin, B.S., Kostamovaara, J.T.: AlGaAs/GaAs asymmetric-waveguide, short cavity laser diode design with a bulk active layer near the *p*-cladding for high pulsed power emission. IET Opotelectron. 15(4), 194–199 (2021). https://doi.org/10.1049/ote2.12033